Electronic Supplementary Material (ESI) for Journal of Materials Chemistry A.

Cation deficiency enables reversal of dopant segregation at perovskite oxide surfaces under anodic potential

Dongha Kim[1]; Adrian Hunt[2]; Iradwikanari Waluyo[2]; Bilge Yildiz[1,3]

[1]*Department of Materials Science and Engineering, Massachusetts Institute of Technology (MIT), Cambridge, USA.*

[2]*National Synchrotron Light Source II, Brookhaven National Laboratory, Upton, NY, USA.*

[3]*Department of Nuclear Science and Engineering, Massachusetts Institute of Technology (MIT), Cambridge, USA.*

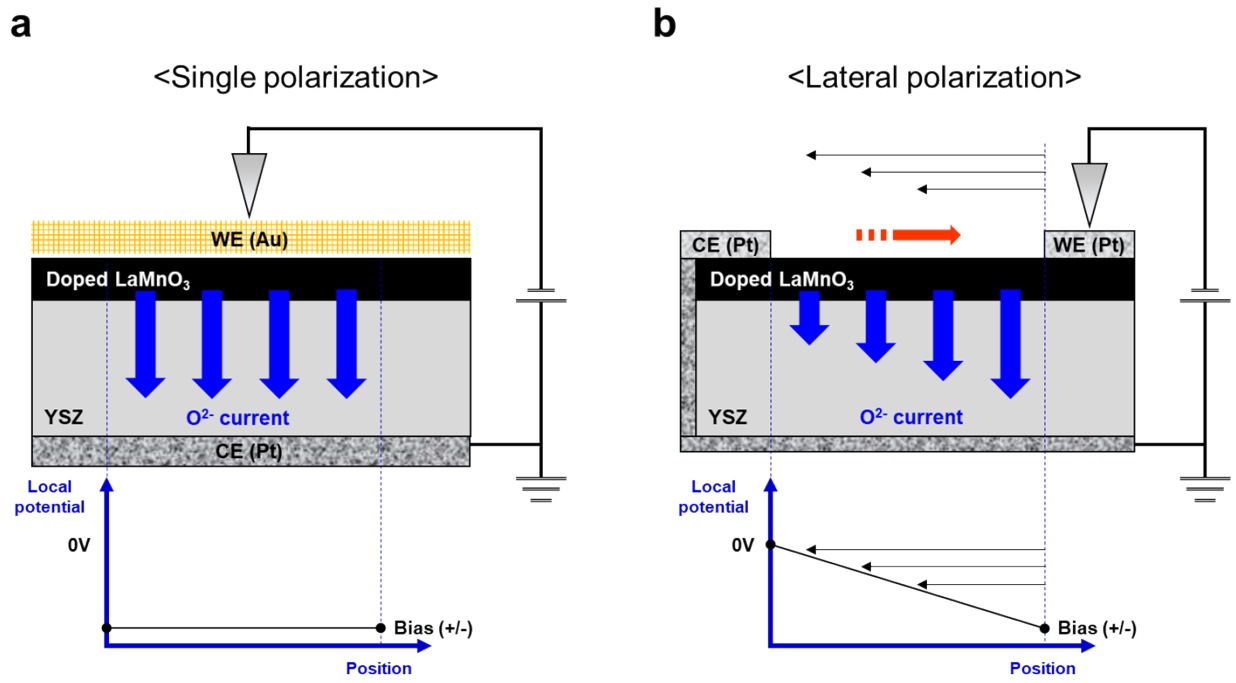

Figure S1. (a) Illustration of the experimental setup for conventional polarization experiment. CE=counter electrode; WE=working electrode; YSZ=Y_2O_3 stabilized ZrO_2, 8% mole Y_2O_3. Au mesh is pressed down by using an alumina screw to ensure a good electrical contact. Single potential is applied uniformly over the doped $LaMnO_3$ (LDM) surface as illustrated in the local potential *vs.* position plot. (b) Illustration of the experimental setup designed for lateral polarization experiment which enables applying a continuous polarization gradient across the top electrode surface. The bias voltage applied between the WE and CE leads to a monotonous decrease in the electrochemical potential applied laterally across the LDM film as illustrated in the potential-position plot.

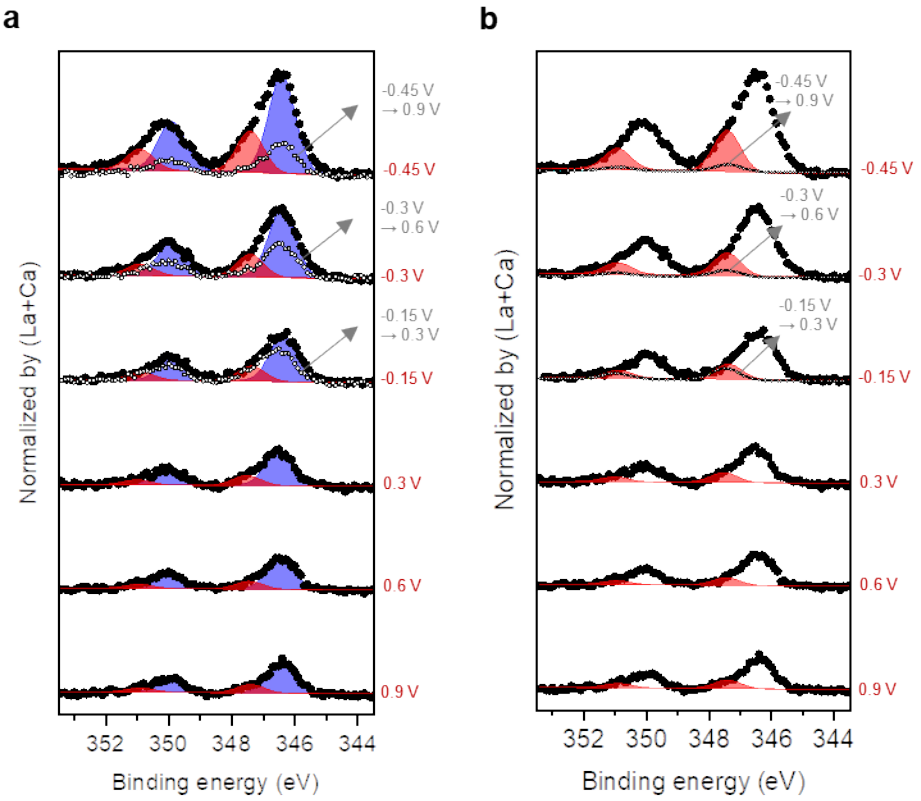

Figure S2. Ca 2*p* core-level XPS spectra of the LCM films annealed with lateral polarization method (**Figure S1b**) at 770˚C in 1 atm O_2. Black filled circles indicate Ca 2*p* spectra from the samples polarized under single potentials and black open circles indicate those polarized with the two-step polarization approach. (a) Each spectrum is deconvoluted into two components, Ca_{latt} (blue, Ca^{2+} in the perovskite phase) and Ca_{surf} (red, Ca^{2+} in the surface CaO_x phase). (b) The same Ca 2*p* spectra as (a) but open circles in this graph indicate the surface component (Ca_{surf}) of Ca 2*p* spectra of the samples annealed with the two-step polarization approach.

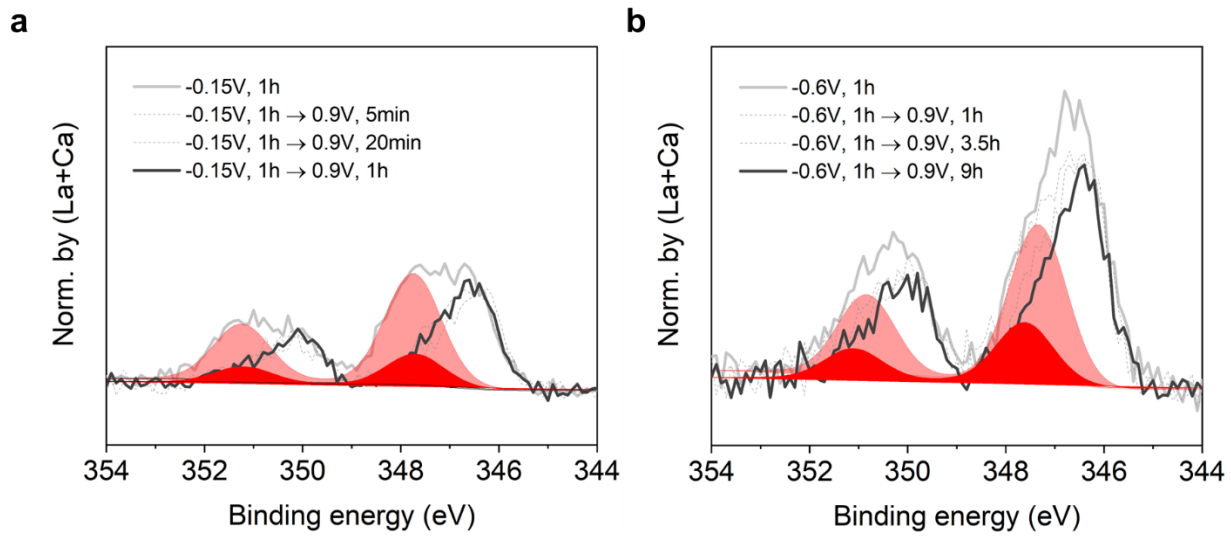

Figure S3. Ca 2*p* XPS spectra of the LCM samples annealed with the two-step polarization approach at 770˚C in 1 atm O_2. (a) Grey line: -0.15 V (1h), dashed black lines: -0.15 V (1h) → +0.9 V (5min, 20min), thick black line: -0.15 V (1h) → +0.9 V (1h). (b) Grey line: -0.6 V (1h), dashed black lines: -0.6 V (1h) → +0.9 V (5min, 20min), thick black line: -0.6 V (1h) → +0.9 V (1h). Faint pink envelopes in (a) and (b) indicate the surface component (Ca_{surf}) of the samples annealed under -0.15 V (1h) and -0.6 V (1h), respectively. Red envelopes in (a) and (b) indicate the surface component (Ca_{surf}) of the samples annealed under -0.15 V (1h) → +0.9 V (1h) and -0.6 V → +0.9 V (9h), respectively.

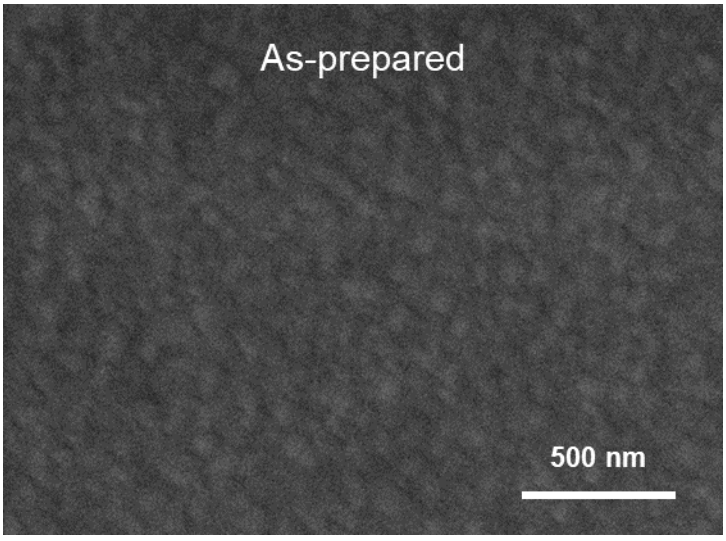

Figure S4. SEM image of the as-prepared LCM film.

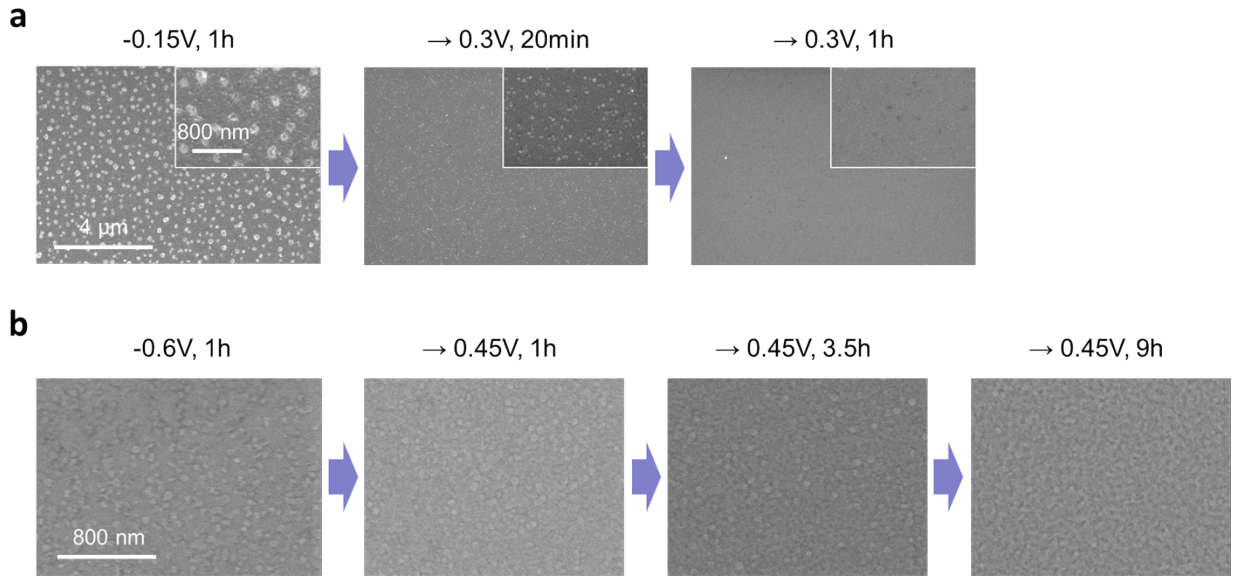

Figure S5. SEM images of the LCM samples annealed with the two-step polarization approach at 770˚C in 1 atm O_2. (a) -0.15 V (1h), -0.15 V (1h) → +0.3 V (20min), and -0.15 V (1h) → +0.3 V (1h). (b) -0.6 V (1h), -0.6 V (1h) → +0.45 V (1h), -0.6 V (1h) → +0.45 V (3.5h), and -0.6 V (1h) → +0.45 V (9h).

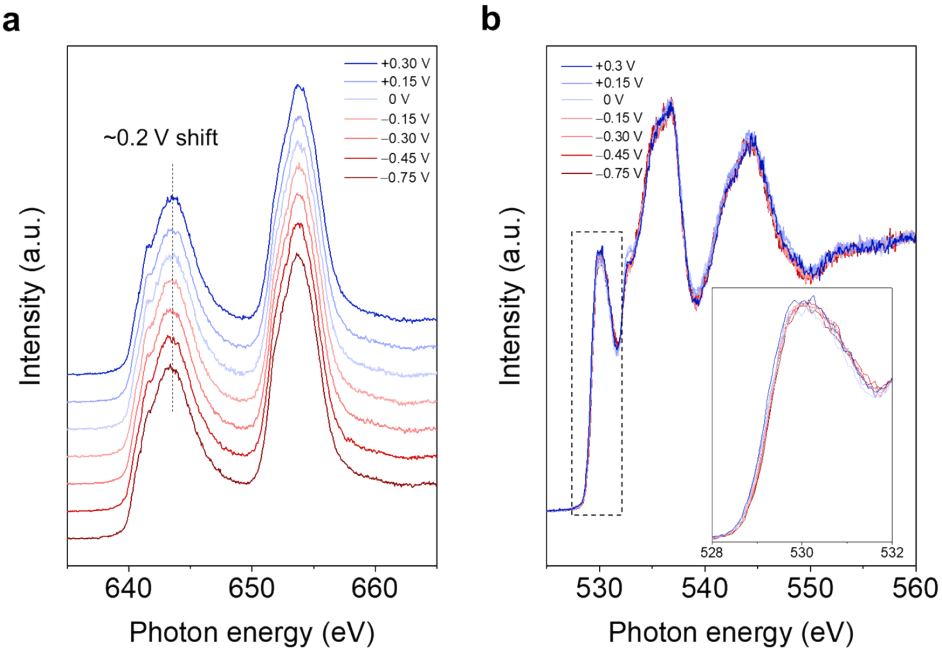

Figure S6. Mn *L*-edge (PFY) (a) and O *K*-edge (PFY) (b) spectra of the LCM samples annealed under different electrochemical potentials at 770˚C in 1 atm O_2 for 1h; -0.75, -0.45, -0.30, -0.15, 0, +0.15, and +0.30 V. Dashed line in (a) indicates the maximum of L_3 peak of the sample kept under +0.30 V. Inset of (b) is a magnified view of the Mn–O hybridization peak (dashed rectangle).

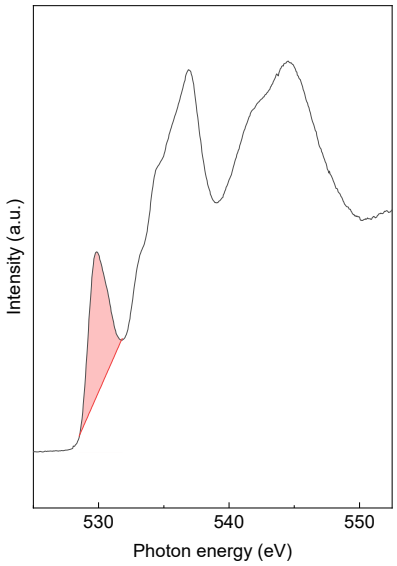

Figure S7. Integrated area (pink shadow) of the Mn–O hybridization peak in the O *K*-edge (TEY) spectrum of the LCM film annealed under 0 V at 770˚C in 1 atm O_2 for 1h.

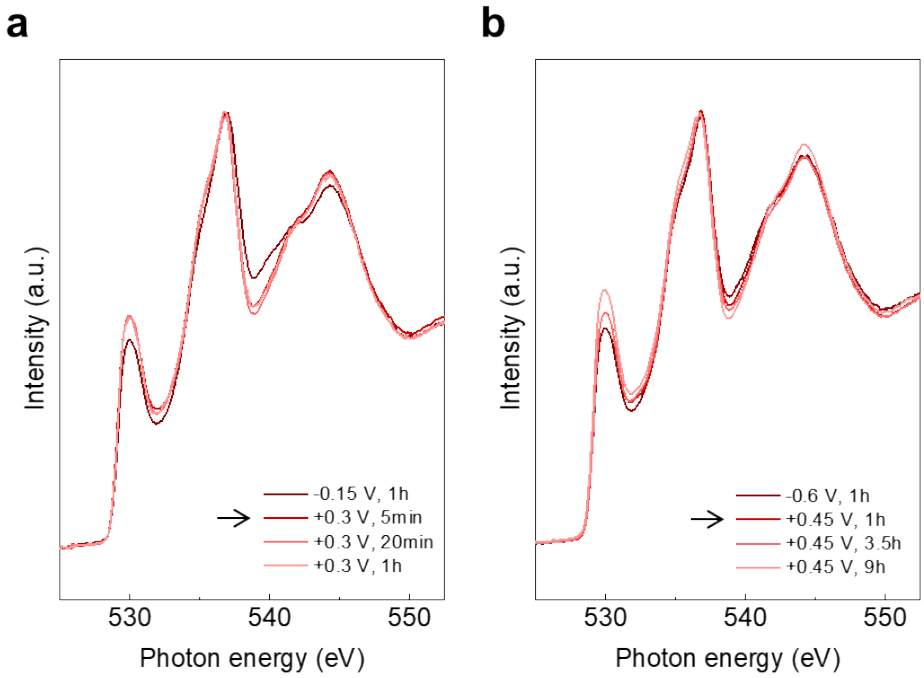

Figure S8. O *K*-edge (TEY) spectra of the LCM samples annealed with the two-step polarization approach under (a) -0.15 V (1h) and -0.15 V (1h) → +0.3 V (5min, 20min, 1h), and (b) -0.6 V (1h) and -0.6 V (1h) → +0.45 V (1h, 3.5h, 9h).

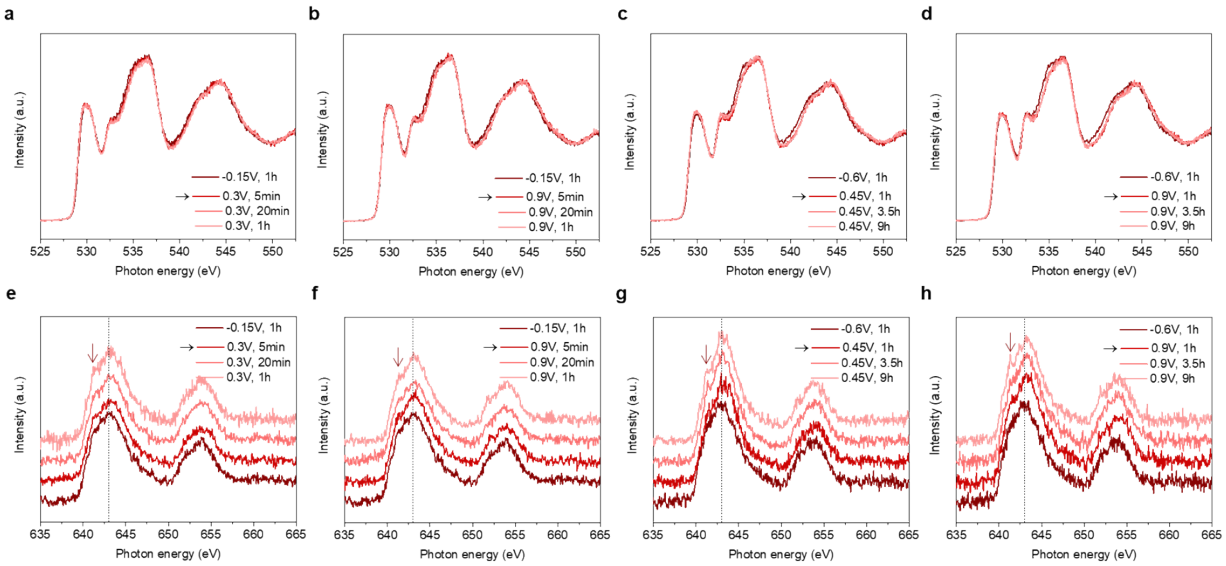

Figure S9. O *K*-edge (PFY) (a ~ d) and Mn *L*-edge (PFY) (e ~ h) spectra of the LCM samples annealed with the two-step polarization approach; (a and e) -0.15 V (1h) and -0.15 V (1h) → +0.3 V (5min, 20min, 1h), (b and f) -0.15 V (1h) and -0.15 V (1h) → +0.9 V (5min, 20min, 1h), (c and g) -0.6 V (1h) and -0.6 V (1h) → +0.45 V (1h, 3.5h, 9h), and (d and h) -0.6 V (1h) and -0.6 V (1h) → +0.9 V (1h, 3.5h, 9h).

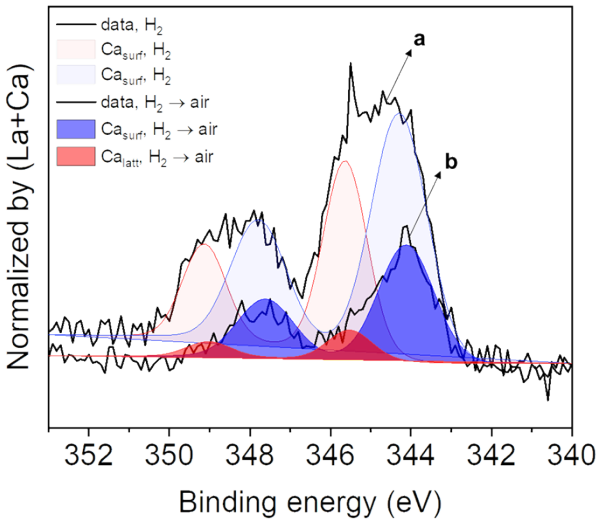

Figure S10. Non-electrochemical dopant re-incorporation reaction. (a) Ca 2*p* XPS spectrum of the LCM sample annealed at 770˚C in 5% H_2/N_2 for 1h and (b) that of the other LCM sample annealed in 5% H_2/N_2 for 1h and sequentially in synthetic air for 3h. Red and blue envelopes indicate the surface (Ca_{surf}) and lattice (Ca_{latt}) components of the two samples, respectively.

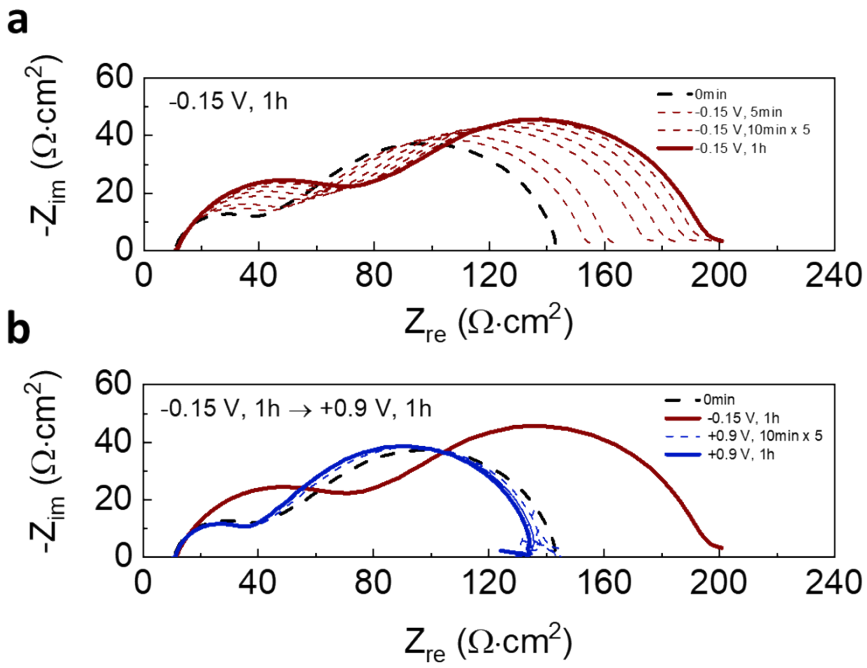

Figure S11. Impedance of LCM film increases under cathodic potential and it decreases under anodic potential. (a) Electrochemical impedance spectroscopy (EIS) spectra of the LCM film taken after annealing it at 770˚C in 1 atm pO_2 under -0.15 V for different time durations. All the EIS spectra were taken at 0 V. Black dashed line: EIS spectrum measured at 770˚C before applying any potential, red dashed lines: after applying -0.15 V (time interval = 5 or 10min), red thick line: after applying -0.15 V for 1h. (b) After applying -0.15 V for 1h, +0.9 V was sequentially applied to the LCM thin film. EIS spectra were measured at 0 V after applying +0.9 V for different time durations. Red thick line: EIS spectrum measured after -0.15 V for 1h, blue dashed lines: after applying +0.9 V for different time durations (time interval = 10min), thick blue line: after applying +0.9 V for 1h.

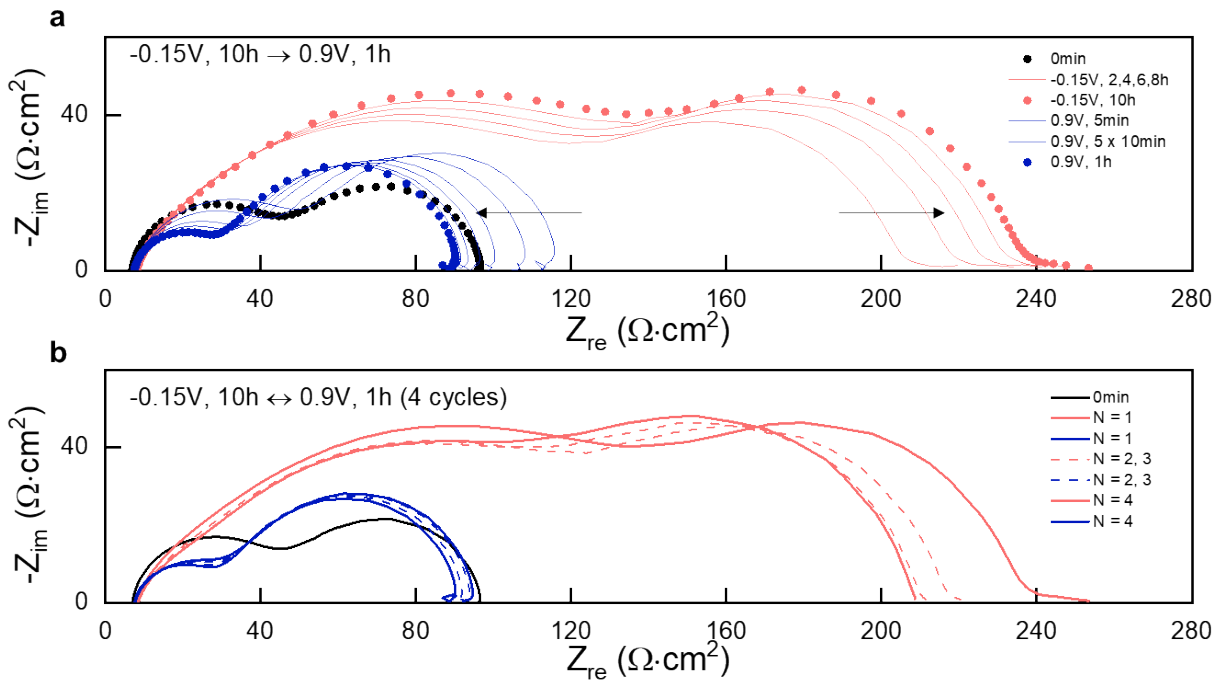

Figure S12. Rapid and reversible activation behavior of LCM under anodic potential. Electrochemical impedance spectroscopy (EIS) spectra of an LCM film taken while annealing it at 770˚C in 1 atm pO_2 under electrochemical potentials. All the EIS spectra were taken at 0 V. (a) An LCM thin film was first annealed under -0.15 V for 10h, followed by annealing under +0.9 V for 1h. The EIS spectra were measured every 2h while applying -0.15 V and 10min while applying +0.9 V. The potential change from -0.15 V to +0.9 V was done in a rate of 1 mV/s. (b) EIS spectra taken during 4 cycles of the same polarization experiments as in (a); one cycle = -0.15 V for 10h and +0.9 V for 1h. The potential change between -0.15 V and +0.9 V was done in a rate of 1 mV/s.

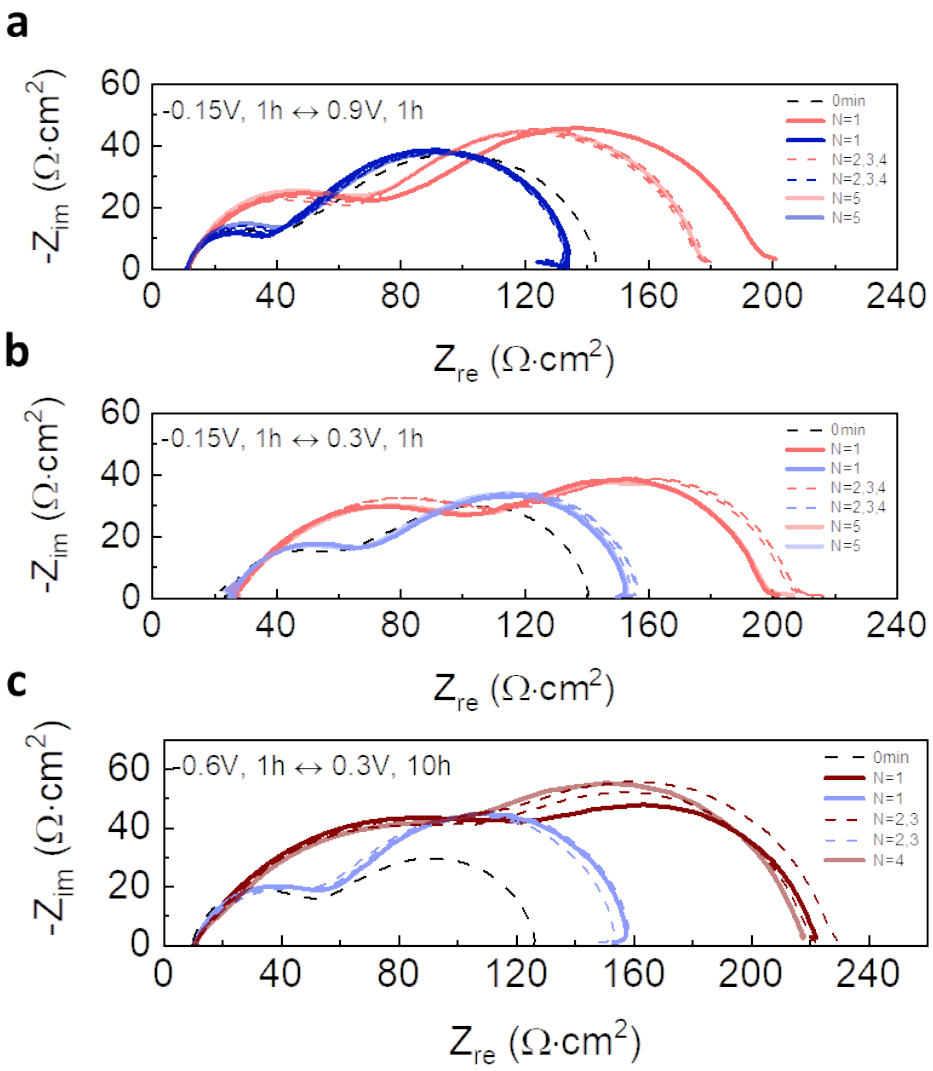

Figure S13. Reversible changes of EIS spectra of LCM films during polarization cycles. Electrochemical impedance spectroscopy (EIS) spectra were measured while annealing LCM films under polarization cycles at 770˚C in 1 atm pO_2. All the EIS spectra were taken at 0 V. The change between cathodic and anodic potentials was done in a rate of 1 mV/s. (a) -0.15 V (1h) ↔ +0.9 V (1h), (b) –0.15 V (1h) ↔ +0.3 V (1h), (c) –0.6 V (1h) ↔ +0.3 V (10h).

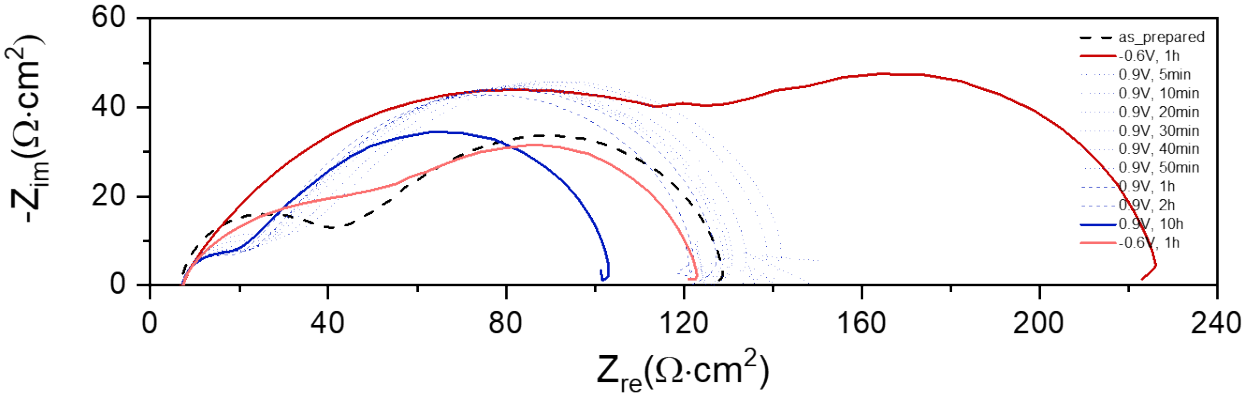

Figure S14. Irreversible changes of EIS spectra of LCM film after a huge potential change. Electrochemical impedance spectroscopy (EIS) spectra were measured while annealing LCM thin films under a polarization cycle at 770˚C in 1 atm pO_2. All the EIS spectra were taken at 0 V. The change between cathodic and anodic potentials was done in a rate of 1 mV/s. After the LCM film undergoes potential change from -0.6 V (1h, red EIS spectrum) to +0.9 V (10h, blue EIS spectrum), its EIS spectrum becomes irreversible (pink EIS spectrum) due to the microstructural changes in it.

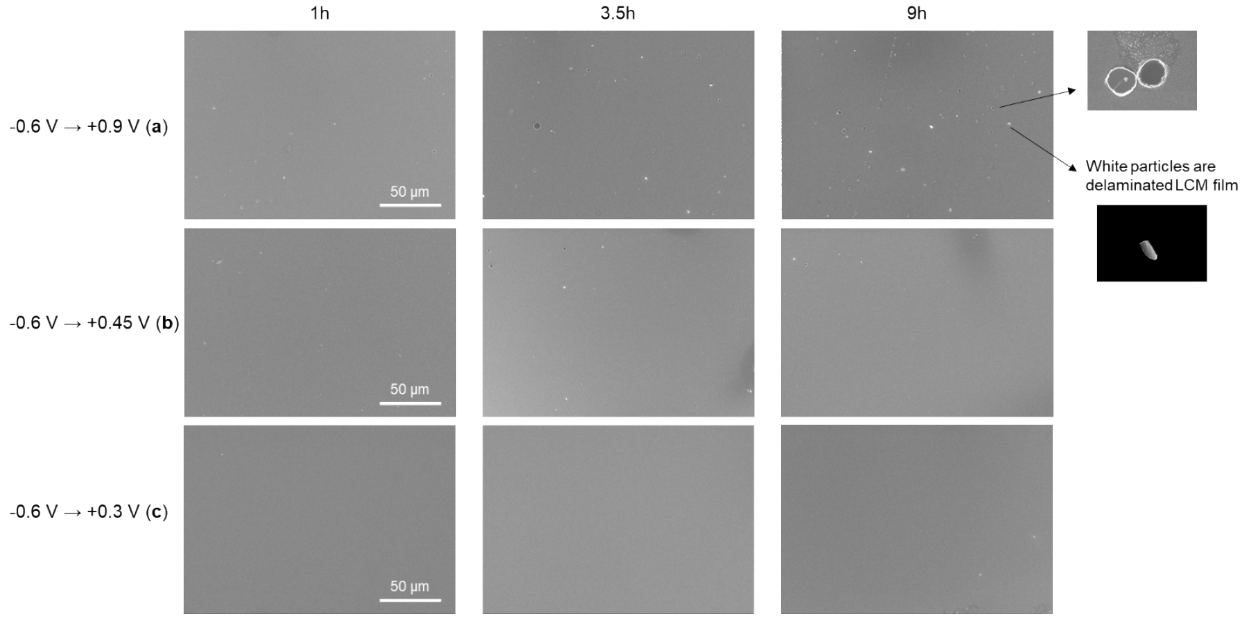

Figure S15. Microstructural changes in the LCM sample which underwent huge potential changes. SEM images of the LCM thin films annealed at 770˚C in 1 atm pO_2 under -0.6 V for 1h and sequentially under (a) +0.9 V, (b) +0.45 V, and (c) +0.3 V for 1h, 3.5h, and 9h. When high anodic potential (+0.9 V) is applied for a long time, LCM thin films start to delaminate as can be seen from the magnified SEM images on the right.

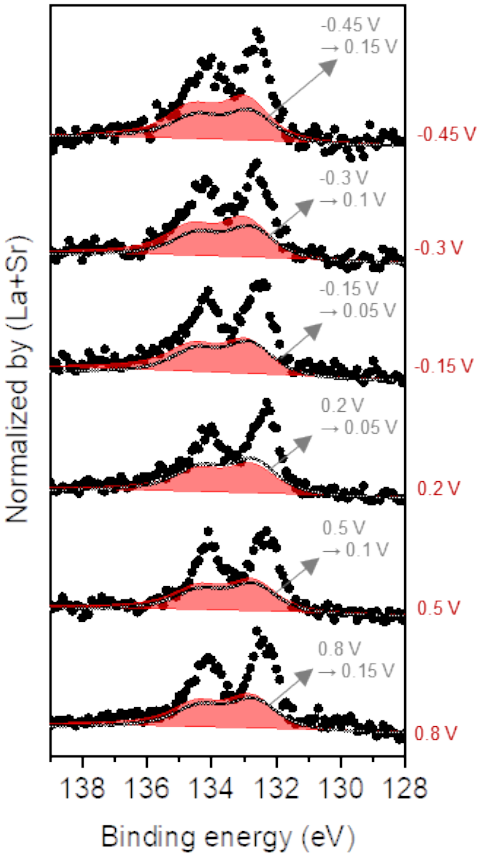

Figure S16. Sr 3*d* core-level XPS spectra of the LSM films annealed with lateral polarization method (**Figure S1b**) at 770˚C in 1 atm O_2. Each spectrum is deconvoluted into two components, Sr_{latt} (Sr^{2+} in the perovskite phase) and Sr_{surf} (red envelopes, Sr^{2+} in the surface SrO_x phase). Black filled circles indicate Ca 2*p* spectra from the samples polarized under single potentials and black open circles indicate the surface component (Sr_{surf}) of Sr 3*d* spectra of the samples annealed with the two-step polarization approach.

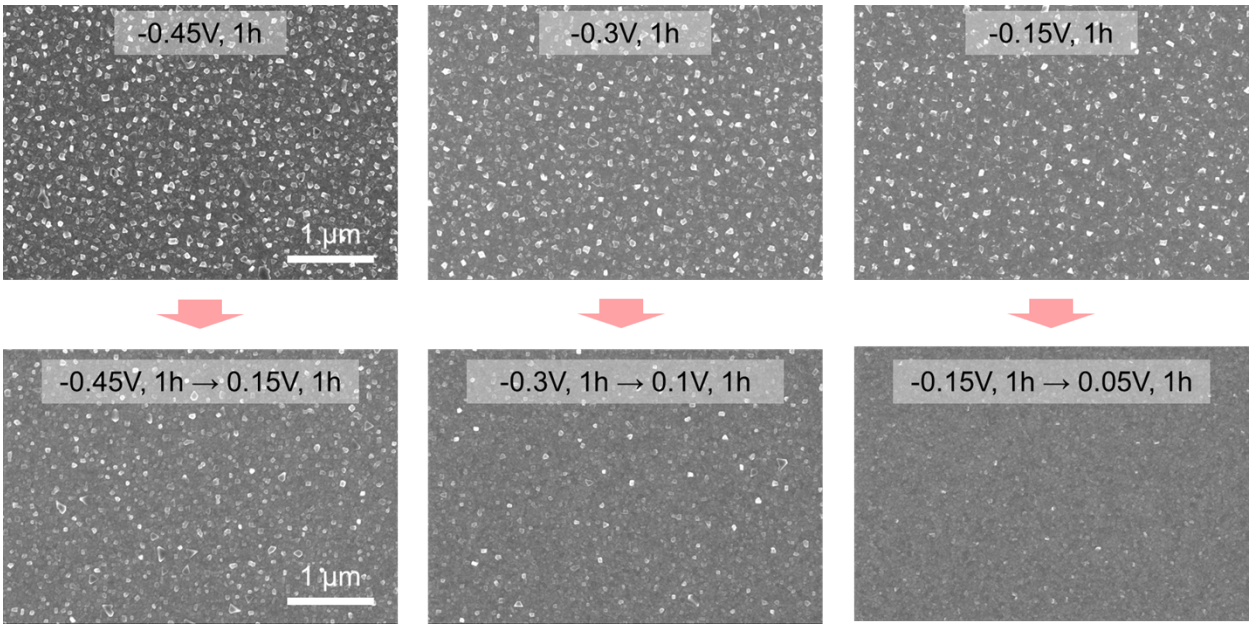

Figure S17. SEM images of the LSM samples (**Figure S16**) annealed under only cathodic potentials for 1h (top) and those annealed first under cathodic potentials for 1h and sequentially under low anodic potentials for 1h (bottom).

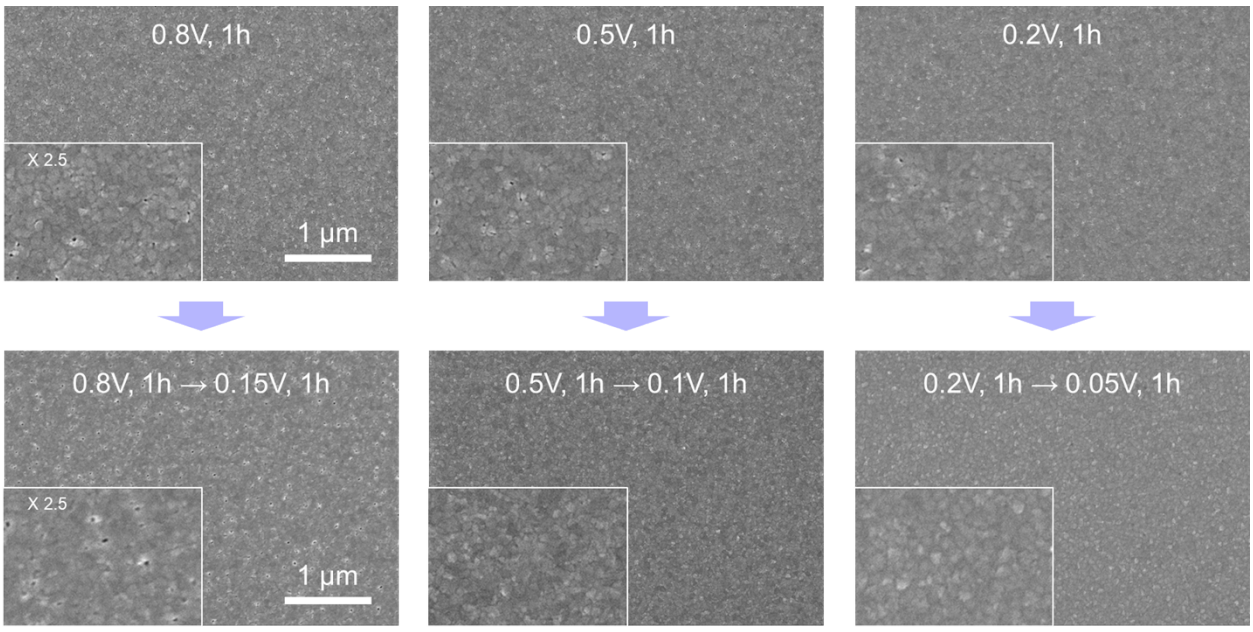

Figure S18. SEM images of the LSM samples (**Figure S16**) annealed under only anodic potentials for 1h (top) and those annealed first under anodic potentials for 1h and sequentially under low anodic potentials for 1h (bottom).

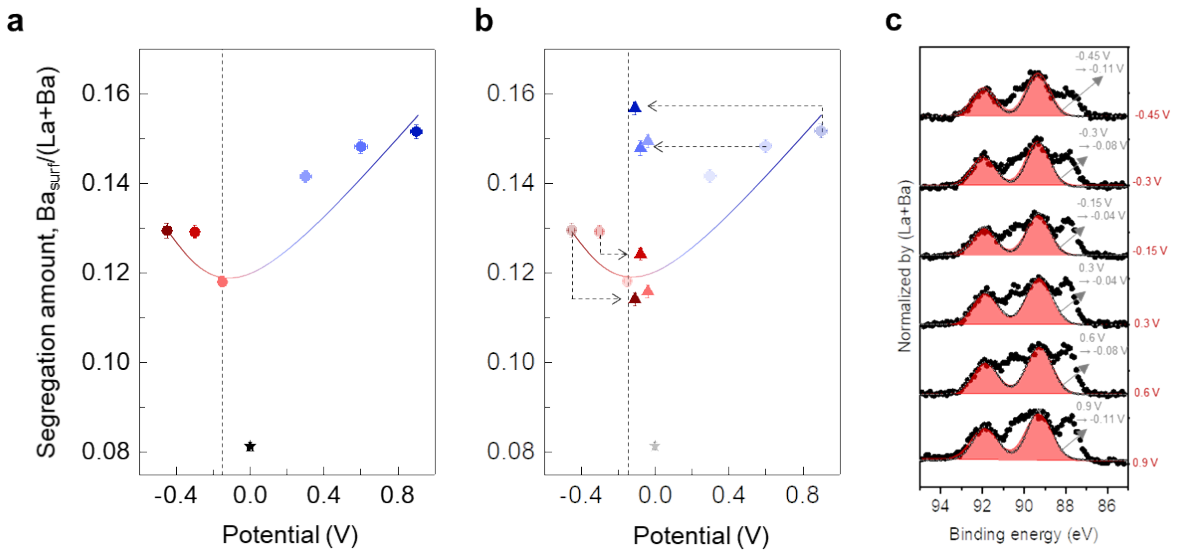

Figure S19. (a) Segregation *vs.* potential graph of $La_{0.8}Ba_{0.2}MnO_3$ (LBM). Thin-film LBM samples were annealed under different potentials at 770˚C for 1h in pure oxygen by using the lateral polarization method (**Figure S1b**). The resulting amount of Ba_{surf} was quantified by XPS and is plotted with respect to the applied potential after normalization with (La+Ba) (circles). The amount of the Ba_{surf} on the as-prepared sample is shown with the star symbol. (b) Another set of LBM samples were annealed with the two-step polarization approach to investigate the reversal of Ba segregation. In this approach, the samples were initially annealed under high cathodic and high anodic potentials for 1h, and sequentially under small cathodic potentials for another 1h; black dashed arrows serve as guides to the eye, indicating the change of potential. The resulting amounts of the Ba_{surf}/(La+Ba) in this set of samples are plotted as triangles. (c) Ba 4*d* core-level XPS spectra of the LBM films. Each spectrum is deconvoluted into two components, Ba_{latt} (Ba^{2+} in the perovskite phase) and Ba_{surf} (red envelopes, Ba^{2+} in the surface BaO_x phase). Black filled circles indicate the Ba 4*d* spectra of the samples polarized under single potentials and black open circles indicate the surface component (Ba_{surf}) of Ba 4*d* spectra of the samples annealed with the two-step polarization approach.

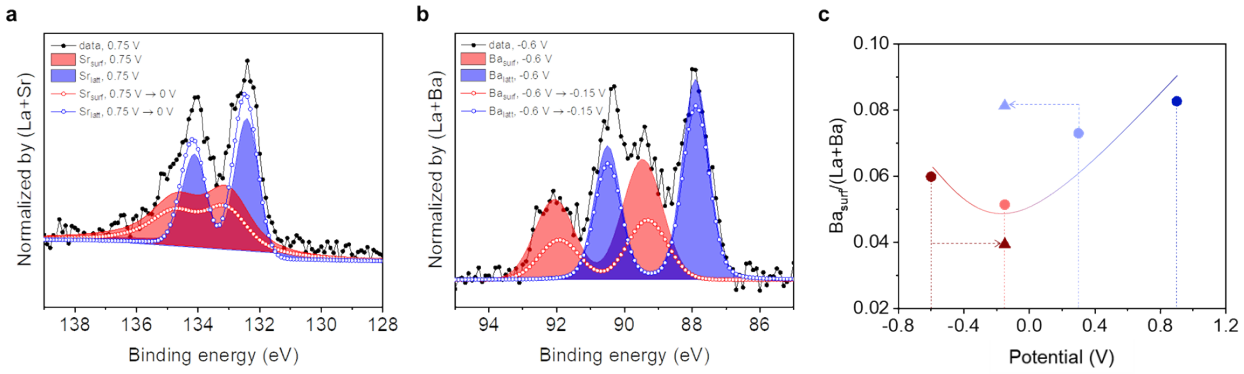

Figure S20. (a) Sr 3*d* core-level XPS spectra from the LSM films annealed with conventional polarization method (**Figure S1a**) at 770˚C in 1 atm O_2. An LSM film was annealed under +0.75 V for 1h and another film was annealed under +0.75 V for 1h and sequentially under 0 V for 1h. The Sr 3*d* spectrum of the LSM film annealed under +0.75 V (black filled circles) is deconvoluted into the surface (blue envelope) and lattice (red envelope) components. Likewise, the Sr 3*d* spectrum of the LSM film annealed under +0.75 V → 0 V is also deconvoluted and the resulting surface and lattice components are plotted as red and blue open circles, respectively. (b) Ba 4*d* core-level XPS spectra from LBM films annealed with conventional polarization method at 770˚C in 1 atm O_2. An LBM film was annealed under -0.6 V for 1h and another film was annealed under -0.6 V for 1h and sequentially under -0.15 V for 1h. The Ba 4*d* XPS spectrum of the LBM film annealed under -0.6 V (black filled circles) is deconvoluted into the surface (blue envelope) and lattice (red envelope) components. Likewise, the Ba 4*d* spectrum of the LBM film annealed under -0.6 V → -0.15 V is also deconvoluted and the resulting surface and lattice components are plotted as red and blue open circles, respectively. (c) Segregation *vs.* potential graph of the LBM films annealed with conventional polarization method at 770˚C in 1 atm O_2. Four LBM films were annealed under single potentials: -0.6 V (1h), -0.15 V (1h), +0.3 V (1h), and +0.9 V (1h), and two LBM films were annealed with the two-step polarization approach under -0.6 V (1h) → -0.15 V (1h) and +0.3 V (1h) → -0.15 V (1h). The resulting Ba_{surf}/(La+Ba) was quantified by XPS and plotted with circles (single potentials) and triangles (two-step polarization approach).

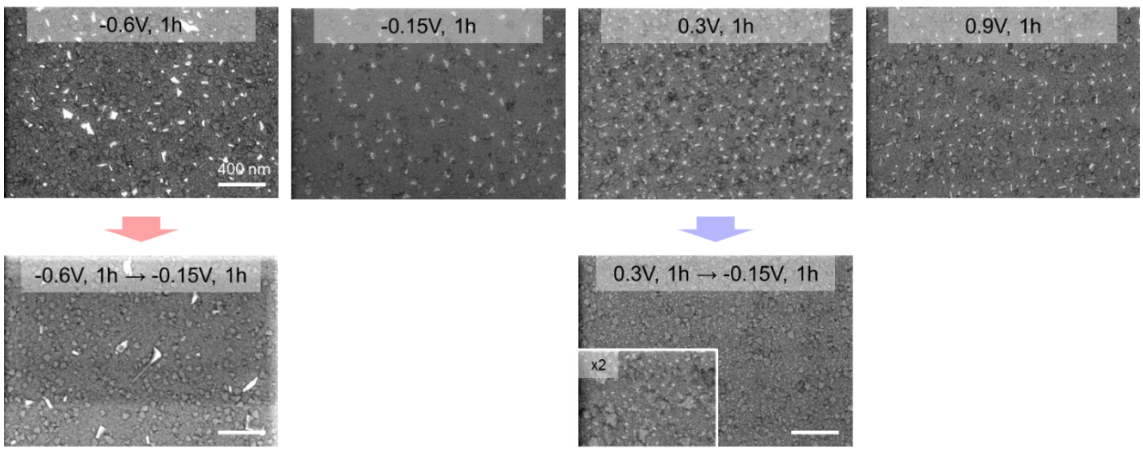

Figure S21. SEM images of the LBM films in **Figure S20c**.

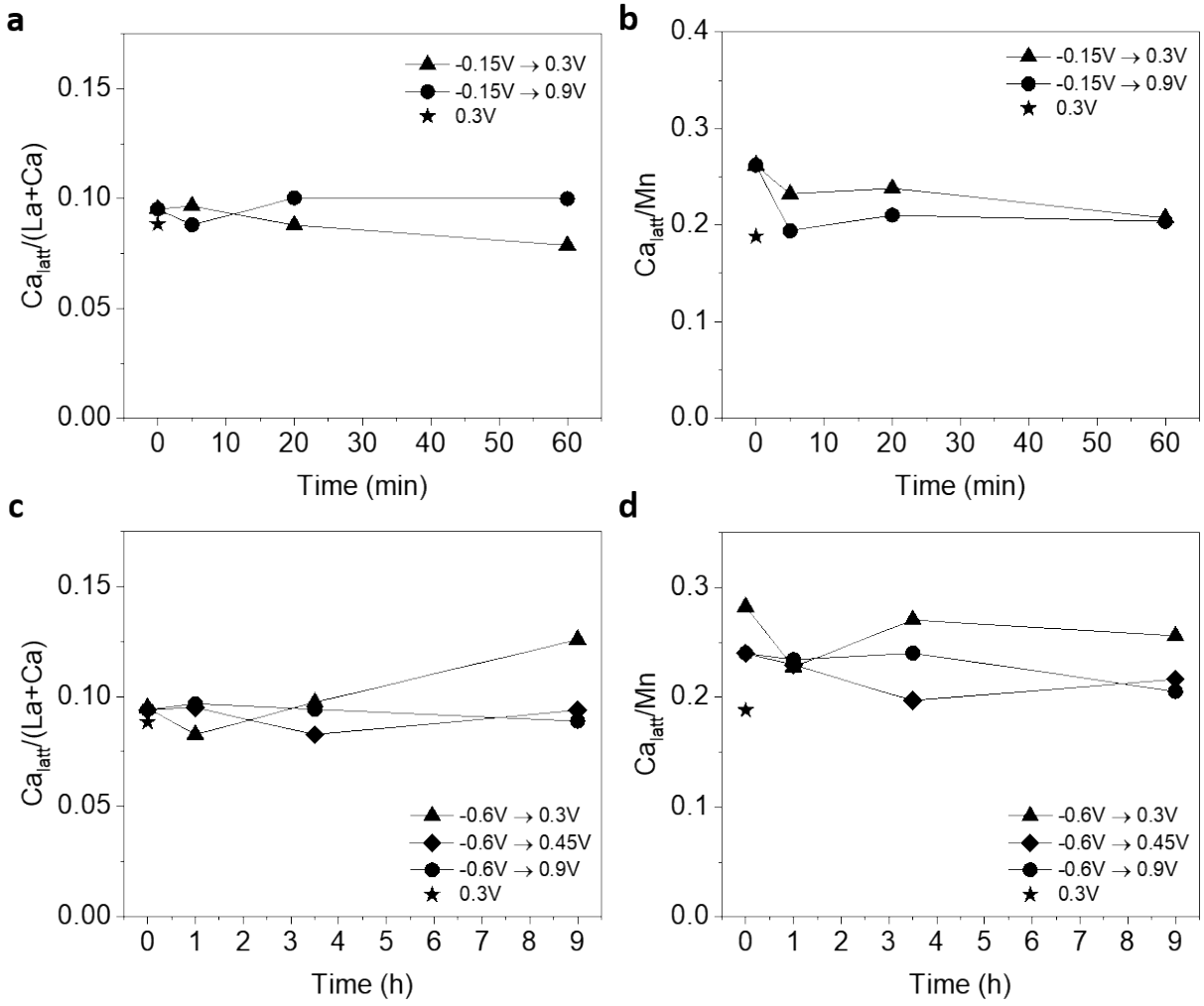

Figure S22. The portion of the lattice component, Ca_{latt}, in the Ca 2*p* XPS spectra of the LCM films annealed with the two-step polarization approach at 770˚C in 1 atm O_2 (**Figure 2**). The amount of Ca_{latt} was normalized by the amount of (La+Ca) (a and c) or Mn (b and d). (a and b) The samples annealed under -0.15 V (1h) → +0.3 V (5min, 20min, 1h) and -0.15 V (1h) → +0.9 V (5min, 20min, 1h), and (c and d) the samples annealed under -0.6 V (1h) → +0.3 V (1h, 3.5h, 9h), -0.6 V (1h) → +0.45 V (1h, 3.5h, 9h), and under -0.6 V (1h) → +0.9 V (1h, 3.5h, 9h). The star symbol indicates the amount of the Ca_{latt} on the reference LCM sample annealed solely under +0.3 V for 1h.

Defect equation of the dopant re-incorporation reaction under anodic polarization

First, the defect equation that corresponds to the oxidation of lanthanum manganites is known as[1]:

$$\text{nil} + 6Mn_B^x + 3/2O_2 \rightarrow V_{La}''' + V_{Mn}''' + 6Mn_B^{\cdot} + 3O_O^x \quad \text{(S1)}$$

Dopant is not included in the reaction for simplicity. Equation S1 shows that cation vacancies are formed as the perovskite oxide is oxidized to satisfy the oxygen-excess non-stoichiometry ($A_{1-\lambda}B_{1-\lambda}O_3 = ABO_{3+\delta}$)[1,2]. During this process, A- and B-site cations migrate to the surface and form new unit cells at the surface. Previous HR-TEM measurement on an oxidized $LaMnO_3$ sample[3] showed that there was no secondary phase at its surface, which implies the formation of the new perovskite unit cells at the surface. For quantitative analysis, Equation S1 can be rewritten as[4]:

$$LaMnO_3 + \frac{\delta}{2}O_2 = (La\square_{\delta/3})(Mn\square_{\delta/3})O_{3+\delta} = \frac{3+\delta}{3}\{(La_{3/(3+\delta)}\square_{\delta/(3+\delta)})(Mn_{3/(3+\delta)}\square_{\delta/(3+\delta)})O_3\} \quad \text{(S2)}$$

Equation S2 shows that new perovskite unit cells with the stoichiometric amount of $\frac{\delta}{3}$ are formed near the surface of the perovskite oxide by incorporating oxygen and forming cation vacancies in the bulk.

$$V_{La}''' + SrO_{surf} + 2Mn_{Mn}^{\cdot} \leftrightarrow Sr_{La}' + 2Mn_{Mn}^X + \tfrac{1}{2}O_2 \quad \text{(S3)}$$

By combining of the dopant re-incorporation reaction (Equation S3) with Equation S1 and considering the fact that oxygen is the surface redox-active species of LCM during oxidation (**Figure 3**), we could formulate the defect reaction for dopant incorporation under anodic polarization as follows:

$$\text{nil} + DO_{surf} + O_O^x + O_2 \leftrightarrow D_{La}' + V_{Mn}''' + 4O_O^{\cdot} \text{ (D = dopant)} \quad \text{(S4)}$$

Reason that LCM bulk undergoes faster oxidation than the surface

Even with the CaO_x layers covering the whole surface of LCM thin film, its bulk could undergo much faster oxidation (**Figure S9**) than its surface. This was because oxygen ions can be supplied from the counter electrode, through YSZ, and finally to the LCM bulk. However, the oxygen could not be supplied up to the surface or near-surface region due to the limited

concentration of oxygen vacancies in the bulk as the LCM film is oxidized. This result implies that the oxidation of LCM bulk and surface occur almost independently.

The reason that applying anodic potential cannot remove the whole CaO_x formed under -0.6 V

Such irreversibility might be because the whole bulk of our LCM thin film could not fully equilibrate with the applied anodic potential. Under -0.6 V, LCM forms a lot of oxygen vacancies in its bulk, and thus the whole bulk of the LCM film would equilibrate with the applied cathodic potential[5,6]. Therefore, Ca would be drawn out from the whole bulk of the LCM film during Ca segregation under -0.6 V. Under anodic polarization, however, LCM has extremely low amount of oxygen vacancies in its bulk, and due to the resulting high resistance, only the near-surface region of the LCM film would equilibrate with the applied anodic potential[5,6]. Therefore, the amount of the new unit cells formed by the oxidation of the LCM film would be low. It may be not enough to accommodate the whole CaO_x formed under -0.6 V.

Strategies to further promote dopant re-incorporation reaction

Figure S23 shows that Sr-doped lanthanum manganite forms a high amount of new unit cells ($\delta/3$, stoichiometric amount) at high $pO_{2,eff}$ when the amount of Sr is low. This means that the amount of the dopant that can be re-incorporated into the new unit cells would also be high. It would also be interesting to investigate dopant re-incorporation reactions on other perovskite oxides which exhibit oxygen-excess non-stoichiometry[8] under oxidizing conditions.

Oxygen-excess non-stoichiometry curve

$$\log pO_2 = \log pO_2^* + \log\left\{\left(\frac{2\delta}{3+\delta}\right)^6\left(\frac{3-17\delta-9x+x\delta}{3+\delta}\right)^{-\frac{2}{3}}\right\} \quad (S5^4)$$

$La_{1-x}Sr_xMnO_3$	T	1/T (K^{-1})	$\log pO_2^*$
x=0.3	770˚C	0.000959	10.7
x=0.2	770˚C	0.000959	7.87
x=0.1	770˚C	0.000959	6.21
x=0	770˚C	0.000959	4.09

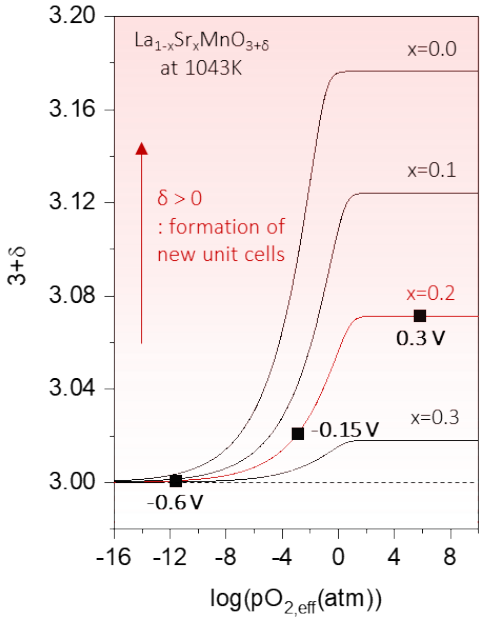

Figure S23. Oxygen non-stoichiometry of $La_{1-x}Sr_xMnO_{3+\delta}$ *vs*. pO_2 graphs. The graphs are drawn by using Equation S5. The value for each parameter in Equation S5 is given in the above table. $\log pO_2^*$ values were obtained from the paper by Mizusaki *et al*[4].

References

1 **Darvish, S., Sabarou, H., Saxena, S. K. & Zhong, Y. Quantitative Defect Chemistry Analysis and Electronic Conductivity Prediction of La0.8Sr0.2MnO3±δPerovskite. *Journal of The Electrochemical Society* 162, E134-E140, doi:10.1149/2.0361509jes (2015).**

2 **Lee, Y. L. & Morgan, D. Ab initio and empirical defect modeling of LaMnO(3+/-delta) for solid oxide fuel cell cathodes. *Phys Chem Chem Phys* 14, 290-302, doi:10.1039/c1cp22380a (2012).**

3 **Van Roosmalen, J. A. M., Cordfunke, E. H. P., Helmholdt, R. B. & Zandbergen, H. W. The Defect Chemistry of LaMnO3±δ: 2. Structural Aspects of LaMnO3+δ. *Journal of Solid State Chemistry* 110, 100-105, doi:https://doi.org/10.1006/jssc.1994.1141 (1994).**

4 **Mizusaki, J. *et al.* Oxygen nonstoichiometry and defect equilibrium in the perovskite-type oxides La1−xSrxMnO3+d. *Solid State Ionics* 129, 163-177, doi:https://doi.org/10.1016/S0167-2738(99)00323-9 (2000).**

5 **Börgers, J. M. & De Souza, R. A. The surprisingly high activation barrier for oxygen-vacancy migration in oxygen-excess manganite perovskites. *Physical Chemistry Chemical Physics*, doi:10.1039/d0cp01281e (2020).**

6 **Brichzin, V., Fleig, J., Habermeier, H. U., Cristiani, G. & Maier, J. The geometry dependence of the polarization resistance of Sr-doped LaMnO3 microelectrodes on yttria-stabilized zirconia. *Solid State Ionics* 152-153, 499-507, doi:https://doi.org/10.1016/S0167-2738(02)00379-X (2002).**

7 **Saranya, A. M. *et al.* Engineering Mixed Ionic Electronic Conduction in La0.8Sr0.2MnO3+δNanostructures through Fast Grain Boundary Oxygen Diffusivity. *Advanced Energy Materials* 5, 1500377, doi:10.1002/aenm.201500377 (2015).**

8 **Peña, M. A. & Fierro, J. L. G. Chemical Structures and Performance of Perovskite Oxides. *Chemical Reviews* 101, 1981-2018, doi:10.1021/cr980129f (2001).**